ISSN 2079-1704. Хімія, фізика та технологія поверхні. 2019. Т. 10. № 3. С. 203-218

PACS: 31.15.A-; 33.25.+k; 33.15.Fm; 82.56.-b; 82.70.Uv doi: 10.15407/hftp10.03.203

V.V. Turov, V.M. Gun'ko, T.V. Krupska, I.S. Protsak, E.M. Pakhlov

STRUCTURAL AND ADSORPTION FEATURES OF AMORPHOUS NANOSILICA MODIFIED BY VARIOUS ADDITION OF POLYMETHYLSILOXANE

Chuiko Institute of Surface Chemistry of National Academy of Sciences of Ukraine
17 General Naumov Str., Kyiv, 03164, Ukraine, E-mail: v_turov@ukr.net

The aim of this study was to elucidate the effects of polymethylsiloxane (PMS) and pretreatment conditions on the behavior of bound water, as well the properties of the PMS/nanosilica blends. Amorphous nanosilica A-300 with addition of PMS hydrogel (PMS/A-300 weight ratio of 1:9 for dry matters) was studied in various dispersion media (air, chloroform alone and with addition of trifluoroacetic acid, TFAA) in comparison to PMS and A-300 alone and PMS/A-300 (1:1) using low-temperature ^{1}H NMR spectroscopy and cryoporometry. Dried nanosilica and PMS alone and in the blends were characterized using microscopy, nitrogen adsorption, infrared spectroscopy, thermogravimetry, and quantum chemistry. It was shown that the properties of the blends depend not only on the components content but also on mechanical treatment causing stronger compaction of the secondary structures of nanoparticles (aggregates of nanoparticles and agglomerates of aggregates) with increasing mechanical loading. Note that a similar behavior of various blends with hydrophobic and hydrophilic nanostructured materials was observed after hydro-compaction under different mechanical loadings. Theoretical modelling shows that the structure of bound water located at a surface of hydrophilic and hydrophobic nanoparticles changes with compaction of aggregates because of changes in the confined space effects and polarity of bound water molecules. These results reflect a general regularity appearing at appropriate amount of added water and certain mechanical loading onto the blends of hydrophilic and hydrophobic nanostructured materials, which become hydrophilic but renew the hydrophobic properties after subsequent drying.

Keywords: *nanosilica, polymethylsiloxane hydrogel, polymethylsiloxane/nanosilica blend, textural and morphological characteristics, mechanical loading effect, interfacial water behavior*

INTRODUCTION

Unmodified and modified amorphous nanosilicas (fumed silicas) are used in various applications in industry, medicine and agriculture [1–5]. Various surface modifications of nanosilica allow one to strongly widen application fields of the materials [3–13]. One of the silica modification ways is the surface hydrophobization by such functionalities as $-Si(R')_{3-m}R_m$ ($R = (CH_2)_nCH_3$), R' = Cl or OR" (R" is a short organic group) [5–7, 10]. Another way deals with adsorption or chemical modifications (*e.g.* hydrophobization) of fumed silica by polymers or polymer fragments [14–24]. The properties of formed polymer shells (*i.e.*, the properties of the final materials) depend not only on chemical structure of polymers but also on their topology (1D, 2D, 3D), cross-linking degree, character of bonding (physical or chemical) to silica surface, intermolecular and intramolecular interactions, as well interactions with water which always is in real systems. The characteristics of the nanosilica/polymer blends depend on preparation conditions (dispersion media, temperature, concentration, mechanical loading, pretreatment time, *etc.*). These conditions can strongly affect the characteristics of the blends depending on a combination of various conditions, *e.g.* certain mechanical loading at certain content of water (or water and polymer). Note that the amounts of linear polymers corresponding to a monolayer coverage of nanoparticles of fumed silica A-300 (with a major fraction of nanoparticles corresponding to 9–10 nm in diameter) are in the range of 8–15 wt. % [19–21].

Poly(di)methylsiloxane (P(D)MS) materials are of importance from a practical point of view [14–19, 25–27]. These materials are used in various applications as components of nanocomposites or co-polymers, surface modifiers, materials for chromatography, components of medicinal preparations, *etc*. For example, PMS hydrogel ($C_{PMS} \approx 7$–10 wt. %) is used as a medicinal oral sorbent Enterosgel

(Kreoma-Pharm, Ukraine) [26, 27]. Note that 3D cross-linked PMS (as a "soft solid"), which has only one CH_3 group attached to each Si atom and a certain amount of residual silanols, strongly differs (in many aspects) from linear PDMS having two CH_3 groups attached to each Si atom [26–32]. The properties of PMS depend strongly on the degree of crosslinking (occurring by condensation of residual silanols from neighboring functional groups) that allows one to prepare hydrophilic PMS as a hydrogel (Enterosgel) or a hydrophobic powder after PMS drying. Clearly, the crosslinking degree increases with increasing temperature and time of drying. Various PMS are of interest from a practical point of view due to their chemical nature, softness, and strong changes in the properties upon drying-wetting-drying [22, 26, 27, 33–42].

A blend of PMS with A-300 was studied at their dry weight ratio $\varphi = 1{:}1$ g/g prepared using dried powders stirred with water at $h = 1$ g/g (as described in detail elsewhere [22]). It is of interest to analyze the behavior of a blend at the amount of PMS close to a monolayer coverage of nanosilica A-300 by linear polymers using the PMS hydrogel (however, PMS is cross-linked one and, therefore, is not linear). Therefore, the aim of this work was to study a blend of A–300/PMS ($\varphi = 9{:}1$ g/g and $h = 1$ g/g), *i.e.*, at $C_{PMS} = 10$ wt. % close to the monolayer coverage of A-300 by linear polymers [19–21] in comparison to initial hydrogel PMS ($h = 13.3$ g/g), A-300 alone, and the PMS/A-300 (1:1) blend ($h = 1$ g/g). To reduce the effect of PMS crosslinking upon drying (due to condensation of residual hydroxyls that transforms PMS into hydrophobic 3D state), the PMS hydrogel ($C_{PMS} \approx 7$ wt. %, $C_{water} \approx 93$ wt. %, PMS is in a hydrophilic state with a minimal degree of cross-linking) was stirred with nanosilica A-300 at their dry weight ratio $\varphi = 1{:}9$ g/g and the degree of hydration at $h \approx 1$ g of water per gram of dry A-300/PMS.

MATERIALS AND METHODS

Initial fumed amorphous nanosilica A-300 (Pilot plant of Chuiko Institute of Surface Chemistry, Kalush, Ukraine) was hydro-compacted (cA-300) using 3 g of water per 1 g of dry A-300, stirred and then dried at room temperature for several days. The bulk density of cA-300 is $\rho_b \approx 0.25$ g/cm^3 instead of 0.05 g/cm^3 for the initial nanosilica.

Commercial polymethylsiloxane (PMS) hydrogel, synthesized using methyltrichlorosilane as a precursor, at ~ 7 wt. % of PMS and 93 wt. % of water (Enterosgel, Kreoma-Pharm, Ukraine) was used as the initial material. In the hydrogel, PMS is hydrophilic because of a relatively small degree of crosslinking caused by condensation of residual silanols. After drying of PMS at room temperature for a week, the amount of water bound in PMS was small (0.7 wt. %) and it became hydrophobic (see [22]). After stirring of dried PMS with water (1:1 g/g) it becomes hydrophilic again and can form uniform suspension [22].

Initial PMS hydrogel and dried hydro-compacted nanosilica A-300 were mixed in a porcelain mortar. The content of PMS in the blend was $C_{PMS} = 10$ wt. % with respect to dry solids. The hydration degree (h) of this blend was 1 g water per gram of dry solids ($h \approx 1$ g/g). If the blend was stirred without any strong mechanical loading (simple mixing) that bulk density $\rho_b \approx 0.66$ g/cm^3 (labelled as PMS/A-300$_{19}$ at the weight ratio $\varphi = 1{:}9$ g/g for dry matters). If the blend was stirred under strong mechanical loading (careful grinding in a porcelain mortar with strong hand-loading giving ~ 20 atm, estimated from the geometry of the mortar and a pestle used and a loading weight, for 15 min) that $\rho_b \approx 0.80$ g/cm^3. This is a hydro-compacted blend labeled as cPMS/A-300$_{19}$ ($\varphi = 1{:}9$ g/g). The blends PMS/A-300$_{19}$ and cPMS/A-300$_{19}$ were compared to initial hydrogel PMS (7 wt. %), as well the PMS/A-300$_{11}$ and cPMS/A-300$_{11}$ blends ($\varphi = 1{:}1$ g/g) (prepared using dried components stirred with water at $h = 1$ g/g) located in different dispersion media (air, $CDCl_3$, and $CDCl_3$ with addition of deuterated trifluoroacetic acid CF_3COOD, TFAA). Hydro-compaction of a set of nanomaterials based on unmodified and modified (hydrophobized) nanooxides was described in detail elsewhere [22, 43–46].

A TEM study was performed using a TECNAI G2 F30 microscope (FEI–Philips, Holland) at the operating voltage of 300 kV. The powder samples were added to acetone (chromatographic grade) and sonicated. A drop of the suspension was then deposited on a copper grid with a thin carbon film. After acetone

evaporation, sample particles remained on the film were studied with TEM.

A SEM study of dried powder samples was performed using a FE–SEM (Hitachi S–4700, Japan) at the operating voltage of 15 kV at the magnification range of 5000–100000.

To analyze the textural characteristics of dried PMS, PMS/A-300_{11}, and A-300 degassed at 453 K for 12 h, low-temperature (77.4 K) nitrogen adsorption–desorption isotherms were recorded using a Micromeritics ASAP 2010 adsorption analyzer. The specific surface area (Table 1, S_{BET}) was calculated according to the standard BET method [47]. The total pore volume (Table 1, V_p) was evaluated from the nitrogen adsorption at $p/p_0 \approx 0.98$–0.99, where p and p_0 denote the equilibrium and saturation pressure of nitrogen at 77.4 K, respectively [48]. The differential ($f_V(R) = dV/dR$) pore size distributions (PSD) were calculated using a nonlocal density functional theory (NLDFT, Quantachrome software) method with a model of cylindrical pores in silica [49]. Incremental PSD (IPSD, $\Phi_V(R_i) = (f_V(R_{i+1}) + f_V(R_i))(R_{i+1} - R_i)/2$ at $\sum\Phi_V(R_i) = V_p$) were calculated using a complex model of pores (such as slit-shaped and cylindrical pores and voids between nanoparticles of silica or polymer, a SCV model) with a self-consistent regularization (SCR) procedure [50].

Low-temperature ^{1}H nuclear magnetic resonance (NMR) spectra of static samples (placed into 4 mm and 5 mm NMR ampoules) of initial PMS hydrogel (h = 13.3 g/g), dry powders hydrated at h = 1.0 g water per gram of dry PMS, A-300, or PMS/A-300 (φ = 1:9 and 1:1 g/g) (preheated at 433 K) were recorded using a Varian 400 Mercury spectrometer (magnetic field 9.4 T, bandwidth 20 kHz) utilizing eight 90° probe pulses of 3 μs duration. Relative mean errors were less than ±10 % for ^{1}H NMR signal intensity for overlapped signals, and ±5 % for single signals; therefore, the average errors in estimations of the amounts of unfrozen water *vs.* temperature are about ±5 %. Temperature control was accurate and precise to within ±1 K. The accuracy of integral intensities was improved by compensating for phase distortion and zero-line nonlinearity with the same intensity scale at different temperatures. To prevent supercooling of water in the samples, the beginning of spectra recording was at 200 K. The samples precooled to this temperature for 10 min were then heated to 280 K at the rate of 5 K/min with steps ΔT = 10 K or 5 K at the heating rate of 5 K/min for 2 min. They were maintained at a fixed temperature for 5 min, and for data acquisition at each temperature, for 1 min. The applications of the low-temperature ^{1}H NMR spectroscopy and NMR cryoporometry, based on the freezing point depression of liquids located in pores depending on the pore sizes, to numerous objects were described in detail elsewhere [19, 51–53]. Note that solids (PMS, silica, ice) do not contribute the ^{1}H NMR spectra recorded here due to a large difference in the transverse relaxation times of liquid water and immobile solid components and due to a narrow bandwidth (20 kHz) of the spectrometer used [19].

The infrared (IR) spectra of PMS and PMS/A-300_{11} were recorded for air-dry samples in the ranges of 4000–1200 cm^{-1} (pellets of 20 mg pressed at 2000 atm) using a Specord M80 (Carl Zeiss). To record the IR spectra, samples with PMS were dried at room temperature for 48 h. The transmittance spectra were recorded with 4 cm^{-1} steps and integration time of 3 s.

The δ_H values for water clusters (up to $100H_2O$) were calculated as the difference in the isotropic values of the magnetic shielding tensors of H atoms ($\sigma_{H,iso}$) of tetramethylsilane, TMS ($\delta_{H,TMS}$ = 0 ppm) as a reference compound (*e.g.* $\sigma_{H,iso}$ = 31.76 and 31.40 ppm for tetra-methylsilane (TMS) by GIAO/B3LYP/6-31G(d,p) and GIAO/ωB97X–D/cc–pVDZ [54], respectively) and a given compound using equation [54]

$$\delta_H = \frac{1}{3} Tr\sigma_{H,TMS} - \frac{1}{3} Tr\sigma_H, \quad (1)$$

where Tr is the trace of matrix, since σ is the tensor with nine elements. The distribution functions of the δ_H values were calculated using a simple equation

$$f(\delta_H) = (2\pi\sigma^2)^{-0.5} \sum_j \exp[-(\delta_j - \delta_H)^2 / 2\sigma^2], \quad (2)$$

where j is a number of H atom, σ^2 is the distribution dispersion, and δ_j is the calculated value of the j-th H atom. Large structures (Fig. 9) were calculated using the PM7 method (MOPAC 2016 package with GPU/CUDA) [55, 56]. To calculate the $f(\delta_H)$ functions using

the PM7 results, a calibration function was used to describe the dependence between atomic charges q_H (PM7) and the δ_H values (GIAO/ωB97X–D/cc–pVDZ) for water clusters ($\delta_H = -27.38435372 + 83.67491184 \times q_H$). This function was used to calculate the ^{1}H NMR spectra of water clusters bound to PMS. Visualization of the calculated structures was carried out using ChemCraft [57] or Avogadro 2 (v. 1.91) [58] program suits.

RESULTS AND DISCUSSION

Mechanical loading affects the distribution of PMS and A-300 nanoparticles in their wetted-dried blends (Figs. 1 and 2), as well the organization of secondary particles and the textural characteristics of the wetted-dried blends or A-300 and PMS alone (Table 1).

Note that PMS nanoparticles (2–4 nm in radius) are smaller than A-300 ones (4–6 nm in radius) [22]. Therefore, the specific surface area of the latter is lower (Table 1, S_{BET}). Additionally, secondary particles of PMS and A-300 are differently organized (Fig. 1 *a*, *b*) due to the formation of chemical bonds between nanoparticles of PMS (upon sol-gel synthesis at room temperature [17, 26, 27]) and mainly physical bonding of silica nanoparticles (flame synthesis at $T > 1200$ K [3–5]). cPMS/A-300$_{11}$ stirred under high mechanical loading demonstrates more compacted secondary structures (Fig. 1 *d*) than that of the blend prepared without strong mechanical loading PMS/A-300$_{11}$ (Fig. 1 *c*). The changes in the organization of secondary particles can strongly influence the confined space effects important for such adsorbates as water, which can be unfrozen in pores at $T < 273$ K [19]. The samples stirred with added water and dried (and degassed before the nitrogen adsorption measurements) demonstrate mainly a mesoporous character (Table 1, V_{meso}, S_{meso} calculated at 1 nm < R < 25 nm in pore radius) with a small contribution of nanopores (V_{nano}, S_{nano} at 0.35 nm < R < 1 nm).

The infrared (IR) spectra (Fig. 3) as well the thermogravimetry data [22] confirm that the amounts of water in air-dried PMS (located in air) are small because it is hydrophobic. Note that water is removed from the initial hydrogel upon heating (TG measurements) up to 200 °C at a maximal evaporation rate at 107 °C [22]. This suggests that a major fraction of water in the hydrogel is bound but with main contribution of weakly bound water (WBW) (*vide infra*).

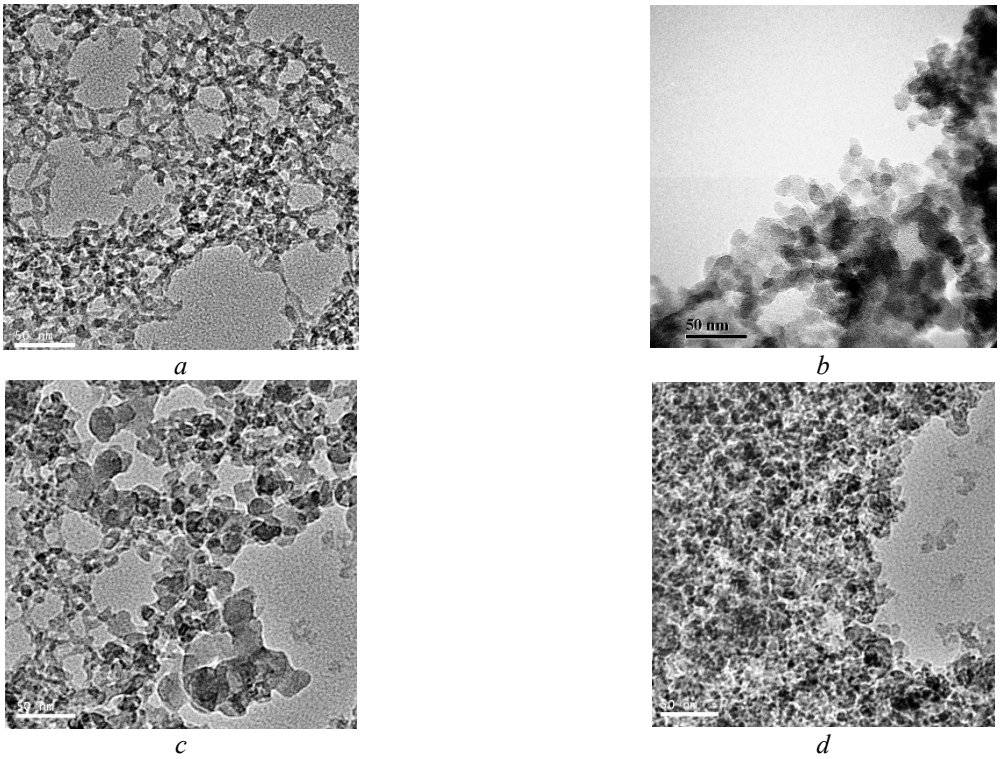

Fig. 1. TEM images of (*a*) PMS, (*b*) A-300, (*c*) PMS/A-300$_{11}$, and (*d*) cPMS/A-300$_{11}$ (scale bar 50 nm)

Table 1. Textural characteristics of dried-degassed PMS alone and PMS/A-300_{11}

Sample	S_{BET}, m^2/g	S_{DFT}, m^2/g	S_{nano}, m^2/g	S_{meso}, m^2/g	S_{macro}, m^2/g	V_p, cm^3/g	V_{nano}, cm^3/g	V_{meso}, cm^3/g	V_{macro}, cm^3/g	$<R_V>$, nm	$<R_S>$, nm
PMS	507	471	2	504	1	1.320	0.002	1.304	0.014	6.08	5.28
Stirred PMS	572	581	1	558	13	2.604	0.001	2.248	0.355	16.86	9.42
PMS/A-300	354	322	35	306	13	1.265	0.019	1.084	0.163	15.25	7.64
cPMS/A-300	407	357	8	399	1	1.021	0.006	1.005	0.011	6.56	5.17
A-300	294	289	44	229	16	0.850	0.023	0.567	0.259	20.41	6.14

Note. The values of V_{nano} and S_{nano}, V_{meso} and S_{meso}, and V_{macro} and S_{macro} were calculated by integration of the $f_V(R)$ and $f_S(R)$ functions at 0.35 nm < R < 1 nm, 1 nm < R < 25 nm, and 25 nm < R < 100 nm, respectively. The values of $<R_V>$ and $<R_S>$ as the average pore radii were calculated as a ratio of the first moment of $f_V(R)$ or $f_S(R)$ to the zero moment (integration over the 0.35–100 nm range) $<R> = \int f(R)RdR/\int f(R)dR$

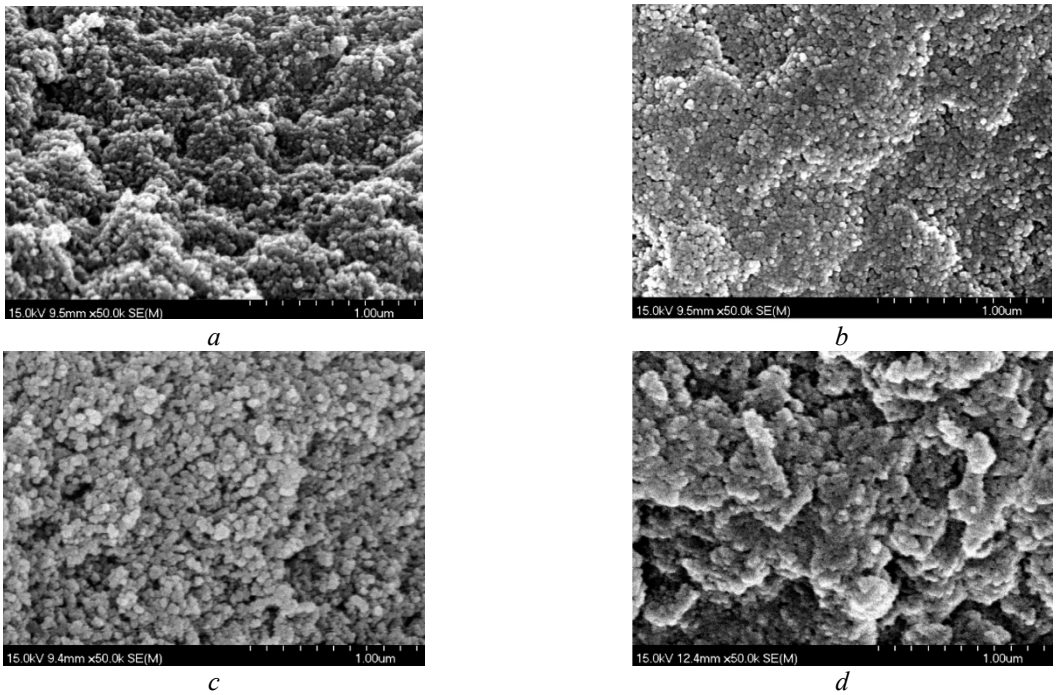

Fig. 2. SEM images of degassed (*a*) Enterosgel, (*b*) PMS dried at room temperature, (*c*) PMS/A-300_{11}, and (*d*) cPMS/A-300_{11} (scale bar 1 μm)

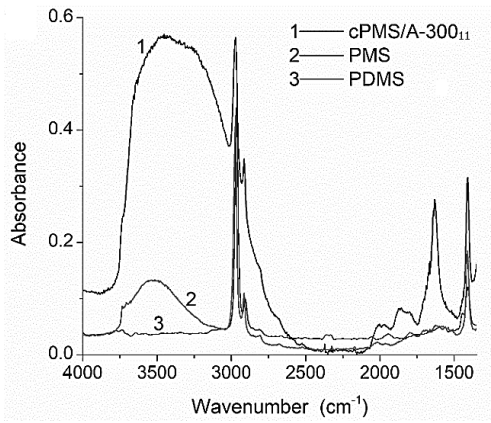

Fig. 3. Infrared spectra of air-dried cPMS/A-300_{11}, PMS, and PDMS alone in the range of 4000–1300 cm^{-1}

Low-temperature (200 K < T < 273 K) ^{1}H NMR spectroscopy of static samples gives additional information on the temperature and interfacial behaviors of water bound in the PMS hydrogel, dried-wetted PMS, initial and compacted A-300, and pretreated PMS/A-300 blends depending on a pretreatment type and dispersion media (Figs. 4–6, Tables 2 and 3). Note that the ^{1}H NMR signal shapes demonstrate certain distortion and asymmetry, especially at low temperatures, due to the presence of various bound water structures (clusters and domains located in voids (pores) of various shapes and sizes), as well nonuniform signal broadening due to nonuniform filling of NMR ampoules by a sample [19, 59].

The ^{1}H NMR spectra of the PMS hydrogel in the chloroform dispersion medium strongly differ from those for the air/water dispersion media (Fig. 4 *a*) since the signals become narrow and intensity faster decreases with decreasing temperature. This suggests that chloroform can displace water from voids in PMS aggregates to form larger domains, which can be frozen at higher temperatures. In other words, contributions of WBW and unbound water (UBW) become larger in the chloroform dispersion medium. This is well visible in the changes in the dependence of the amount of unfrozen water (C_{uw}) *vs* temperature (Fig. 5 *a*). Note that changes in pretreatment of PMS (drying, wetting, stirring) and dispersion media composition affect the ^{1}H NMR spectra [22] and changes in contents of WBW (frozen at 260 K < T < 273 K) and strongly bound water, SBW (frozen at T < 260 K), as well strongly (SAW at δ_H = 4–6 ppm) and weakly (WAW at δ_H = 1–2 ppm) associated waters [19]. Note that only SAW is observed for the PMS hydrogel and hydrated PMS/A-300$_{19}$ (Fig. 4).

The interfacial and temperature behaviors of water bound in PMS/A-300$_{19}$ (Fig. 4 *b–d*) or PMS/A-300$_{11}$ [22] at h = 1 g/g become more complex in comparison to those for PMS alone (Fig. 5 *a*).

This is caused by the difference in the interactions of water with PMS and nanosilica (due to the difference in their surface structure), as well by the organization of water clusters and domains in various voids between different nanoparticles (Fig. 7). For example, in the chloroform medium, besides main signal at δ_H = 4.5–5.5 ppm (Fig. 8 *a*, s1), there is an additional signal at 7.3-7.7 ppm appearing at low temperature (Fig. 8 *a*, s2). The latter corresponds to SBW/SAW.

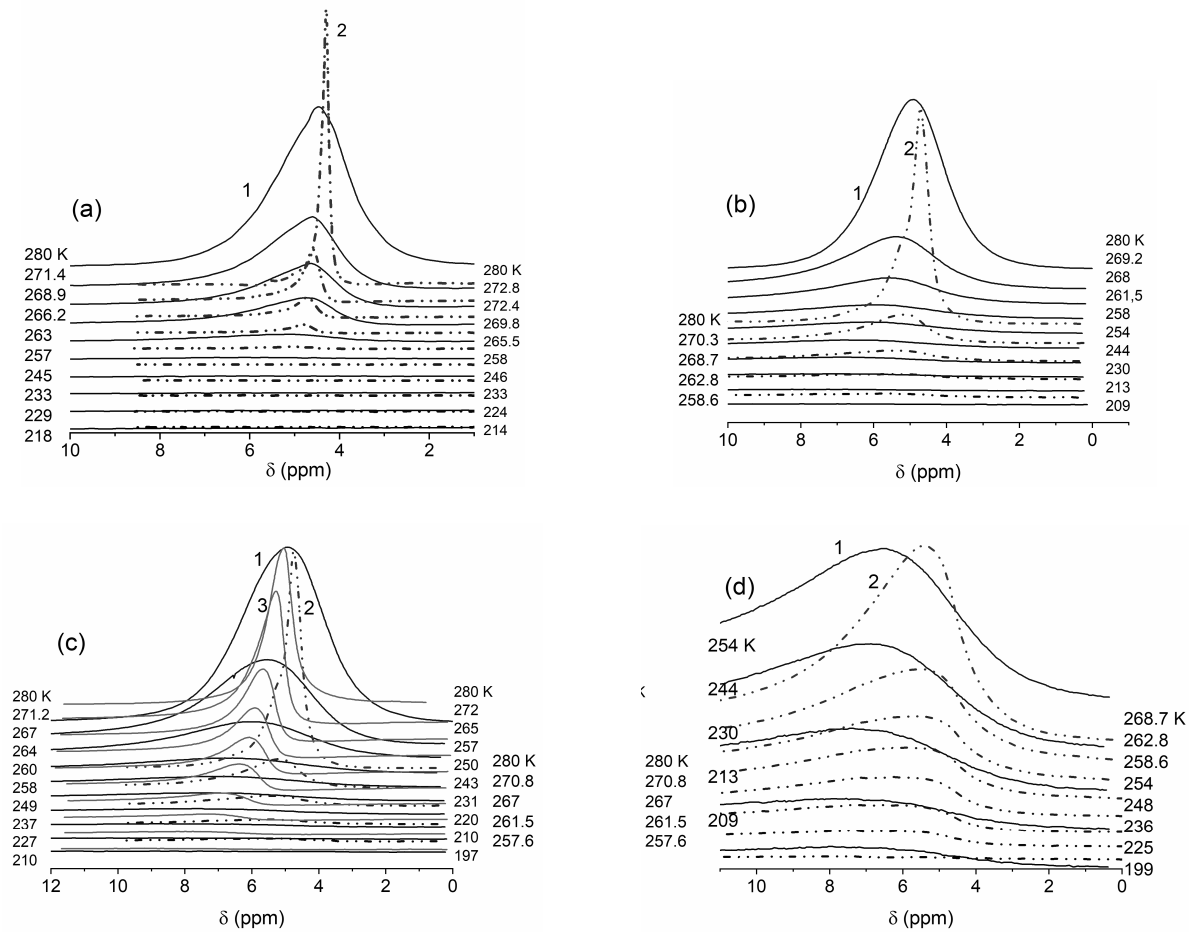

Fig. 4. ^{1}H NMR spectra recorded at different temperatures for (*a*) initial PMS hydrogel in air (1, solid lines) and $CDCl_3$ (2, dotted-dashed lines); (*b, d*) PMS/A-300$_{19}$ at h = 1 g/g in air (1, solid lines) and $CDCl_3$ (2, dotted-dashed lines) (*d*) shows the spectra at low temperatures; (*c*) cPMS/A-300$_{19}$ at h = 1 g/g in air (1, solid lines), $CDCl_3$ (2, dotted-dashed lines), and $CDCl_3$/TFAA (7:1) (3, solid lines)

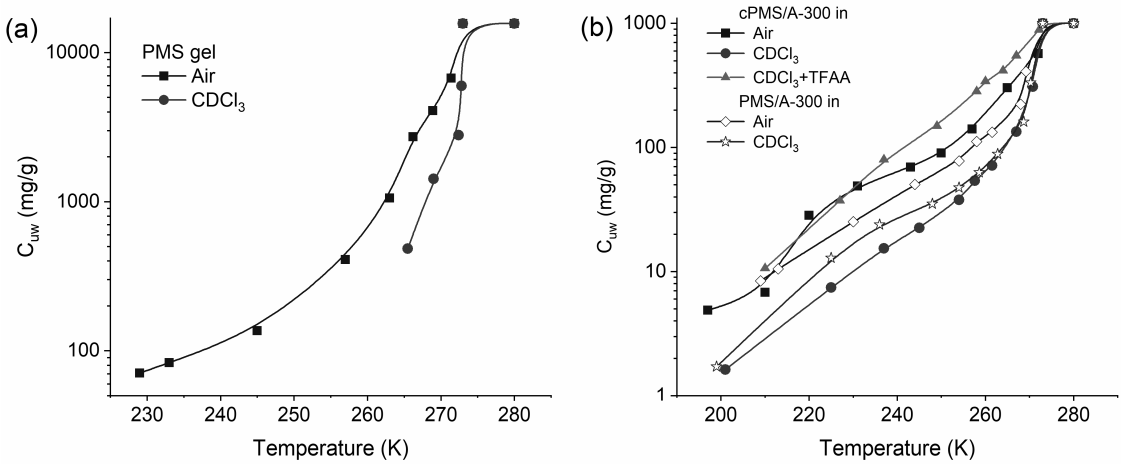

Fig. 5. The amounts of unfrozen water (C_{uw}) *vs* temperature for (*a*) initial PMS hydrogel in air and $CDCl_3$; (*b*) cPMS/A-300_{19} and PMS/A-300_{19} at h = 1 g/g in air, $CDCl_3$, and $CDCl_3$/TFAA (7:1)

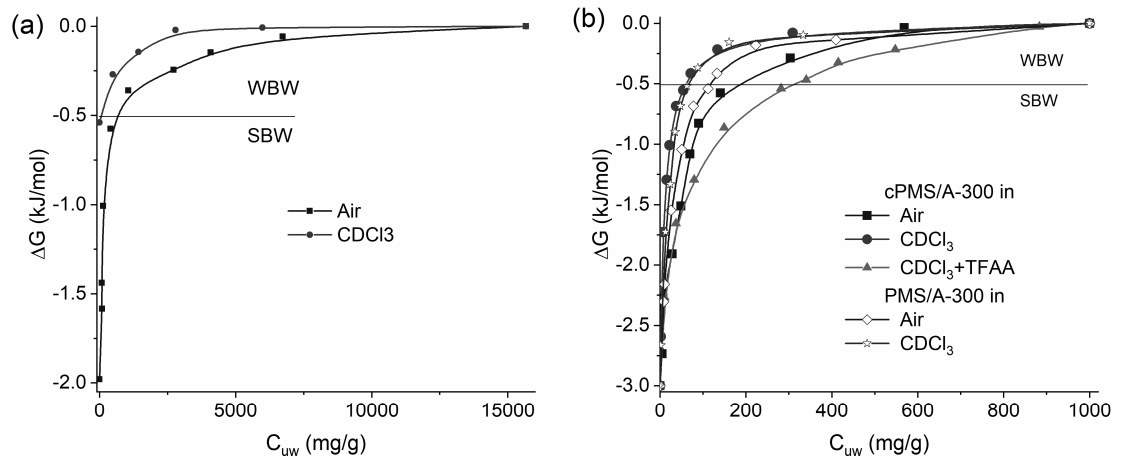

Fig. 6. Relationships between the amounts of unfrozen water (C_{uw}) and changes in the Gibbs free energy (ΔG) of this water depending on temperature for (*a*) initial PMS hydrogel being in air or chloroform medium, and (*b*) PMS/A-300 (1:9) blend hydrated at h = 1 g/g with high mechanical loading (cPMS/A-300_{19} at bulk density ρ_b = 0.8 g/cm^3) and low mechanical loading (PMS/A-300_{19} at ρ_b = 0.66 g/cm^3) being in air, chloroform or $CDCl_3$+TFAA (7:1) dispersion media

Addition of TFAA affects the δ_H values and freezing temperature due to the colligative properties [60] of the acid solution (Fig. 2 *c*, lines 3). However, the δ_H values are smaller than that observed for pure TFAA solution at $\delta_H \approx 11$ ppm characteristic for strong acids [59]. This effect could be explained by reduced activity of bound water as a solvent [19]. In other words, bound water can poorly dissolve even TFAA.

The amount of SBW in the initial PMS (7 wt. %) hydrogel is $C_{uw}^s = 0.7$ g per gram of dry PMS (Table 2). In the chloroform medium, the C_{uw}^s value strongly decreases because chloroform can displace water from voids between PMS nanoparticles to reduce the contact area between immiscible liquids [19]. In the hydrogel, the total content of water $h \approx 13.3$ g/g is greater than the amounts of SBW+WBW (Table 1, C_{uw}^s+C_{uw}^w) both for chloroform or air dispersion media because a fraction of water is unbound water (UBW), which is frozen at $T \approx 273$ K. Addition of chloroform affecting the bound water organization leads to a decrease in the values of γ_S (as a modulus of total changes in the Gibbs free energy of bound water), amounts of SBW (C_{uw}^s) and WBW(C_{uw}^w), specific surface area in contact with bound unfrozen water in mesopores ($S_{meso,uw}$), average radius of unfrozen water clusters located in mesopores $\langle R_{meso,uw} \rangle$, and to an increase in the average melting

temperature of ice (Tables 2 and 3, $<T_m>$). Similar effects in the re-organization of bound unfrozen water in the chloroform dispersion medium are observed for PMS/A-300 (Tables 2 and 3). However, a much lower value of $h = 1$ g/g (instead of 13.3 g/g) results in disappearing of UBW. Therefore, addition of chloroform reduces the C_{uw}^{s} value and enhances contribution of WBW (Tables 2 and 3, C_{uw}^{w}). However, these changes depend on the pretreatment type of the blends.

For strongly treated cPMS/A-300_{19} ($h = 1$ g/g) located in air, the C_{uw}^{s} value is greater than that for PMS/A-300_{19} (Table 2) that corresponds to greater values of γ_S, $S_{nano,uw}$, $S_{meso,uw}$ and lower values of $<T_m>$, $<R_{nano,uw}>$, $<R_{meso,uw}>$, despite the $V_{meso,uw}$ value is smaller. However, in the chloroform medium, the values of C_{uw}^{s} and γ_S decrease stronger for cPMS/A-300_{19}, but a diminution of the $V_{meso,uw}$ value is smaller than that for PMS/A-300_{19}. The character of these changes is well observed in changes in the PSD (Fig. 7 *c*) and IPSD (Fig. 7 *d*) corresponding to the size distribution of unfrozen water located in various pores (voids between nanoparticles). In contrast to the PMS hydrogel (Fig. 7 *a*, *b*), changes in the PSD and IPSD are more complex for composite systems. The re-organization of nanoparticles in secondary structures during strong mechanical loading (Figs. 1 and 2) affects the interfacial and temperature behaviors of bound water due to changes in the size distributions of voids; *i.e.*, the confined space effects change.

Changes in the $<T_m>$ and γ_S values (Tables 2 and 3, Fig. 9) give clear pictures on the strength of interactions of unfrozen water with surroundings depending on several factors such as adsorbent composition, water content, pretreatment type, and dispersion medium. However, there is no linear or monotonic correlations between the $<T_m>$ and γ_S values because the former is determined from the $C_{uw}(T)$ function, but the latter is determined from the $\Delta G(T)$ function, and the relationship between the $C_{uw}(T)$ and $\Delta G(T)$ functions is not linear (Figs. 5 and 6). The maximum γ_S value is observed for the initial PMS hydrogel.

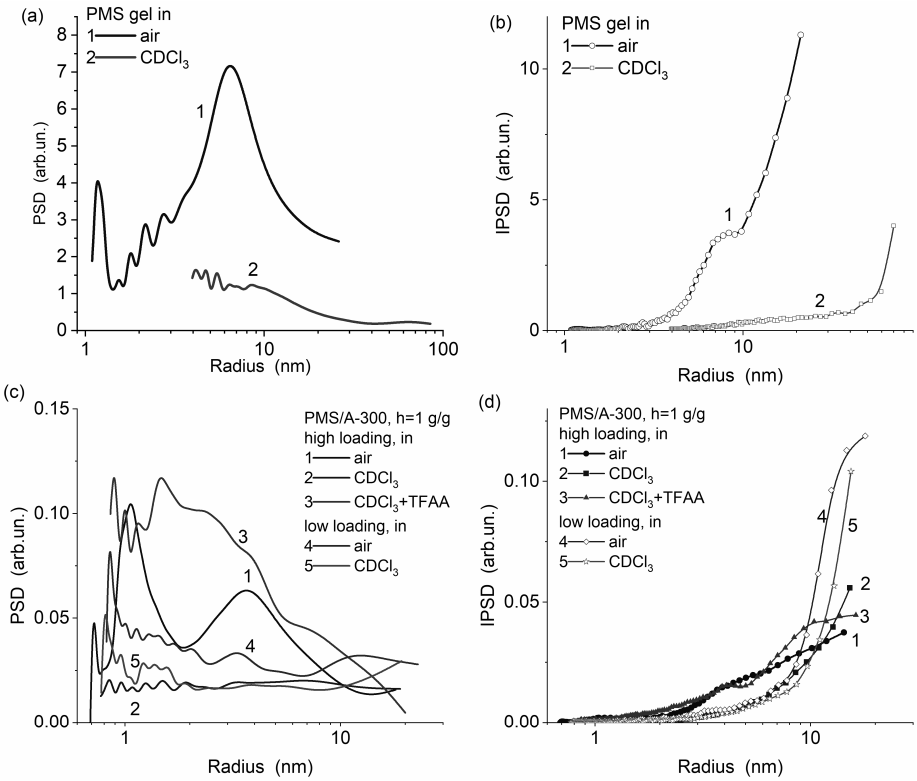

Fig. 7. (*a, c*) Differential and (*b, d*) incremental size distributions of pores (voids between nanoparticles) filled by unfrozen water for (*a, b*) initial PMS hydrogel in air and $CDCl_3$; (*c, d*) cPMS/A-300_{19} and PMS/A-300_{19} at $h = 1$ g/g in air, $CDCl_3$, and $CDCl_3$/TFAA (7:1)

Table 2. The characteristics of bound water unfrozen at T< 273 K for PMS and blends with PMS/A-300_{19} treated at low and high mechanical loading

Sample	Medium	C_{uw}^{s}, mg/g	C_{uw}^{w}, mg/g	$-\Delta G_s$, kJ/mol	γ_S, J/g	$\langle T_m \rangle$, K	$S_{nano,uw}$, m²/g	$S_{meso,uw}$, m²/g	$S_{macro,uw}$, m²/g	$V_{nano,uw}$, cm³/g	$V_{meso,uw}$, cm³/g	$V_{macro,uw}$, cm³/g	$\langle R_{nano,uw} \rangle$, nm	$\langle R_{meso,uw} \rangle$, nm	$\langle R_{macro,uw} \rangle$, nm
PMS gel	Air/water	700	5767	2.04	113.1	265.35	0	576	0	0	6.467	0		22.46	
	$CDCl_3$	100	4230	0.58	30.2	268.91	0	248	52	0	2.122	2.098		17.08	80.59
PMS/A-300_{19}	Air	125	875	2.82	13.6	263.20	23	61	0	0.010	0.600		0.91	19.78	
Low loading	$CDCl_3$	65	935	3.17	9.0	262.62	18	34	0	0.008	0.307		0.89	17.88	
cPMS/A-300_{19}	Air	200	800	2.93	17.5	256.35	29	64	0	0.013	0.467		0.90	14.47	
High loading	$CDCl_3$	60	940	2.86	7.9	262.42	9	33		0.004	0.283		0.90	16.96	
	$CDCl_3$+ TFAA	300	700	2.55	26.2	256.68	32	93		0.015	0.732		0.93	15.69	

Note. C_{uw}^{s} and C_{uw}^{w} are the amounts of weakly and strongly bound waters; ΔG_s is the changes in the Gibbs free energy of water layer closely located to a surface; γ_S is the modulus of the total changes in the Gibbs free energy of bound water unfrozen at T< 273.15 K; $\langle T_m \rangle$ is the average melting temperature; $S_{nano,uw}$ and $V_{nano,uw}$, $S_{meso,uw}$ and $V_{meso,uw}$ are the specific surface area and pore volume of nanopores at 0.2 nm <R< 1 nm and mesopores at 1 nm <R< 25 nm, respectively, in contact with unfrozen water

Table 3. Characteristics of water (h = 1.0 g/g) bound to non-compacted and compacted PMS alone and with A-300 (φ = 1:1) in air, chloroform medium alone or with addition of TFAA, and hydro-compacted nanosilica cA-300

Sample	Medium	C_{uw}^{s}, mg/g	C_{uw}^{w}, mg/g	$-\Delta G_s$, kJ/mol	γ_S, J/g	$\langle T_m \rangle$, K	$S_{nano,uw}$, m²/g	$S_{meso,uw}$, m²/g	$V_{nano,uw}$, cm³/g	$V_{meso,uw}$, cm³/g
PMS	Air	280	720	2.48	25.13	258.63	138	98	0.056	0.758
PMS	$CDCl_3$	10	990	2.44	0.69	262.36	3	1	0.001	0.007
PMS	$CDCl_3$/TFAA	475	525	2.45	27.73	257.39	15	226	0.006	0.796
cA-300*	Air	40	1085	2.41	7.22	268.1	4	48	0.002	0.710
cA-300*	$CDCl_3$	30	1095	2.53	6.10	268.4	10	44	0.005	0.626
PMS/A-300	Air	115	885	2.85	12.06	257.04	64	86	0.026	0.297
PMS/A-300 (SAW)	$CDCl_3$	95	25	3.04	2.88	251.26	20	14	0.008	0.041
PMS/A-300 (WAW)	$CDCl_3$	795	95	2.77	9.91	257.88	52	54	0.021	0.202
cPMS/A-300	Air	225	775	2.68	17.45	261.78	110	70	0.044	0.675
cPMS/A-300	$CDCl_3$	30	970	2.90	5.01	263.69	31	20	0.012	0.207

Note. C_{uw}^{s} and C_{uw}^{w} are the amounts of weakly and strongly bound waters; ΔG_s is the changes in the Gibbs free energy of water layer closely located to a surface; γ_S is the modulus of the total changes in the Gibbs energy of bound water unfrozen at T< 273.15 K; $\langle T_m \rangle$ is the average melting temperature; $S_{nano,uw}$ and $V_{nano,uw}$, $S_{meso,uw}$ and $V_{meso,uw}$ are the specific surface area and pore volume of nanopores at R< 1 nm and mesopores at 1 nm <R< 25 nm, respectively, in contact with unfrozen water. *h = 1.125 g/g

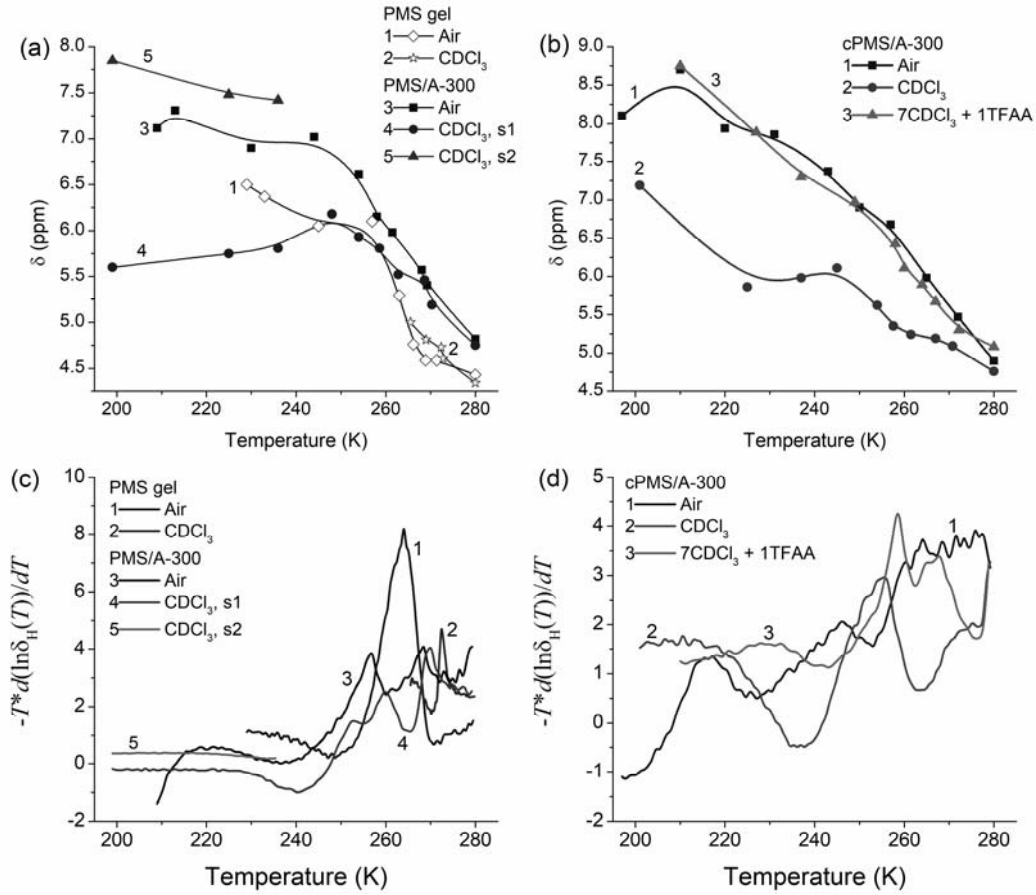

Fig. 8. Chemical shifts δ_H of unfrozen water in the ^{1}H NMR spectra of (*a*) PMS hydrogel and PMS/A-300$_{19}$ in air and $CDCl_3$; (*b*) cPMS/A-300$_{19}$ at $h = 1$ g/g in air, $CDCl_3$, and $CDCl_3$/TFAA (7:1) *vs*. *T*, and (*c, d*) corresponding entropy functions $s(T) = -T(\partial(\ln\delta(T))/\partial T)_P$ *vs T*

Any treatment or addition of chloroform, a decrease in water content or addition of nanosilica results in a decrease in the γ_S value; *i.e.*, the integral interactions of water with surrounding decrease. One of the main factors of this general effect is a decrease in the surface area of contacts between water and polar functionalities of solids (*e.g.*, $S_{meso,uw}$ (Table 2) is maximal for the initial PMS hydrogel). Note that PMS is hydrophilic in the initial hydrogel (due to residual silanols) in contrast to dried PMS, in which a number of residual silanols decreases due to condensation that results in the hydrophobic properties of the dried powder [22]. The second important factor is that the specific surface area of hydrated, dried, stirred-dried PMS is much greater than that of initial or hydro-compacted A-300 (Table 1). Therefore, the same amounts of A-300 nanoparticles can interact with a smaller amount of water than that for the PMS nanoparticles.

Note that dried PMS is mainly mesoporous with a very small contribution of nanopores (Table 1). Therefore, at $h = 1$ g/g, chloroform can strongly displace water from PMS that results in a minimal value of γ_S (Fig. 9, Tables 2 and 3). However, wetting of air-dried PMS results in appearance of nanopores (Table 3, $S_{nano,uw}$). Chloroform can displace this water from nanopores; therefore, the $S_{nano,uw}$ value strongly reduces. In the case of hydro-compacted cA-300 alone, the effects of chloroform is lower, and the $S_{nano,uw}$ value even increases from 4 to 10 m^2/g, and $S_{meso,uw}$ decreases only slightly (from 48 to 44 m^2/g). For PMS/A-300$_{11}$ (Table 3) and PMS/A-300$_{19}$ (Table 2) at $h = 1$ g/g, the chloroform effects on bound water are greater than that for A-300 alone (Tables 2 and 3, Figs. 4–6, 9).

For the values of δ_H, there is a general tendency in an increase in δ_H with decreasing temperature (Fig. 8 *a*, *b*). This is due to several

reasons such as decreasing mobility of the molecules tending to spatial positions corresponding to them in ice (for ice Ih $\delta_H \approx 7$ ppm but for bulk water $\delta_H \approx 4.5$–5.5 ppm), ordering water structure with decreasing contribution of interstitial water; and decreasing vibrational and rotational mobility of the bonds and functional groups. However, there are such additional factors affecting the δ_H (T) course as changes in surroundings with appearing nonpolar co-adsorbate/dispersion medium, changes in the pore (void) topology depending on adsorbent composition, formation of ice crystallites in pores that affects the pore shape. These effects lead to nonlinear δ_H dependence on temperature because the mentioned above factors depend differently on temperature. Note that for PMS/A-300_{19} and cPMS/A-300_{19}, WAW (δ_H = 1–2 ppm) is practically absent (Figs. 4 and 8) in contrast to the PMS/A-300_{11} blends [22]. This effect can be explained by a smaller content of the hydrophobic functionalities with decreasing content of PMS in the blends because water at a mosaic hydrophobic/hydrophilic surfaces can be present the WAW form [19, 61, 62].

Melting of ice crystallites (with an endothermic effect) leads to increased entropy of the system. Changes in the entropy of bound water/ice ($s(T)$) demonstrate several peaks (Figs. 8 *c*, *d*) due to the presence of several types of ice/bound water structures. The position of these peaks depends on several factors (water content, confined space effects – PSD, organization of PMS and A-300 nanoparticles in aggregates and agglomerates of aggregates, dispersion media type, presence of TFAA). Smaller h and pore sizes or addition of TFAA result in the $s(T)$ peak shift toward lower temperatures, but the chloroform appearance gives the opposite effect. As a whole, these changes are in agreement with changes in the γ_S values.

Theoretical calculations (Fig. 10) show that interactions of water clusters with hydrophobic PMS functionalities (corresponding to hydrophobic hydration [63–65]) are weaker than those with silanols or other water molecules. This result corresponds to a tendency of the formation of larger water structures (clusters, domains) upon interaction with hydrophobic surroundings. However, for the water shell around a non-dehydrated PMS particle (119 structural units with 60 OH groups), the ^{1}H NMR spectrum is similar to that for the shell around the dehydrated PMS particle (with residual 9 OH groups). This effect is due to the clusterization of the water shells for both particles that can result in the appearance both of SAW and WAW structures in the adsorption layer. Interaction energy (ΔE_t) in the system with dehydrated PMS particle (119 structural units with residual 9 OH groups) surrounded by a water shell clustered is ΔE_t = –19.1 kJ/mol per a water molecule. The interaction between the water shell and PMS particle (per a water molecule) gives ΔE_t = –7.1 kJ/mol, but in the water shell *per se*, it is stronger ΔE_t = –12.0 kJ/mol.

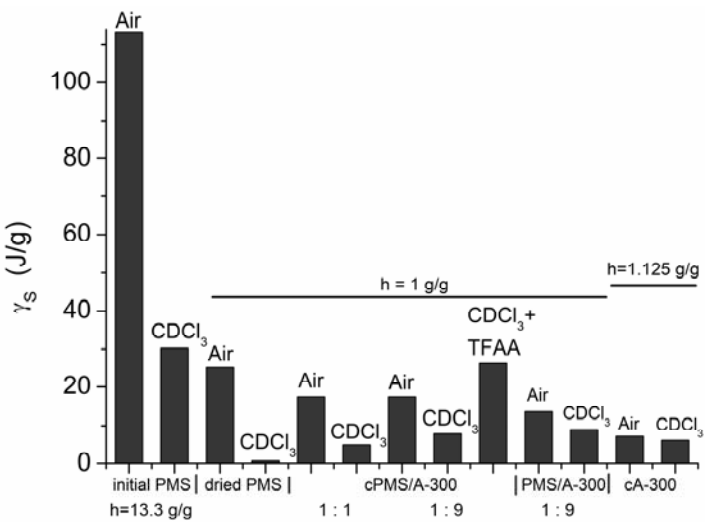

Fig. 9. Changes in the γ_S values of bound water depending on adsorbent composition, water content, pretreatment type, and dispersion medium

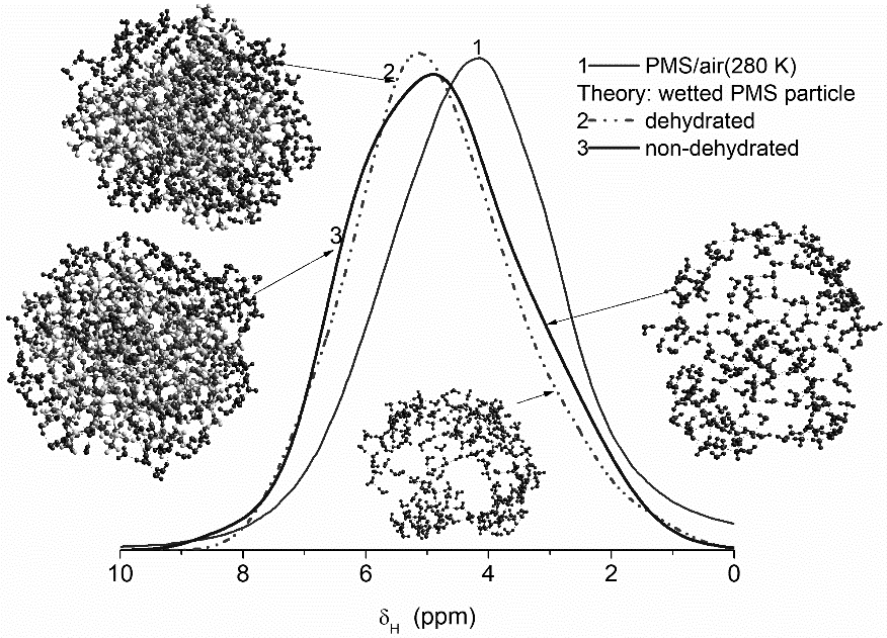

Fig. 10. Experimental ^{1}H NMR spectrum of water bound to PMS (h = 1 g/g) in air (curve 1) and theoretical spectra calculated (using the PM7 method and the calibration function) for wetted dehydrated (2, with residual 9 OH groups) and non-dehydrated (3, with residual 60 OH groups) PMS particles (~2.7 nm in diameter) with 119 tetrahedra with a clustered hydration shell

CONCLUSION

Drying of initial PMS hydrogel results in the formation of a hydrophobic powder. However, the powders of dried hydrophobic PMS alone or in a blend with hydrophilic nanosilica can be easily rehydrated upon stirring with water at h = 1 g/g. The properties of the blends depend on the components content and mechanical treatment due to stronger compaction of the PMS/A-300 secondary structures with increasing mechanical loading. Note that a similar behavior of the blends with hydrophobic and hydrophilic nanostructured materials was observed for several compositions [22, 32, 43–46] as well the effects during hydro-compaction [56] that reflect in a general regularity appearing at appropriate amounts of added water and certain mechanical loading onto the blends of hydrophilic and hydrophobic nanomaterials. This pretreatment results in the reorganization of the secondary structures and removal of micro-scaled air bubbles bound to hydrophobic components in an initial mixture wetted. Note that after drying of wetted-stirred blends, the powders can demonstrate the hydrophobic properties, which however disappear after subsequent wetting-stirring.

A fraction of water bound to initial PMS (h = 13.3 g/g) or dried-wetted PMS (h = 1 g/g) or dried-wetted PMS/A-300 (h = 1 g/g) located in air corresponds to strongly bound water frozen at T < 260 K, but practically entire water is strongly associated and characterized by the chemical shift at δ_H = 4.5–5.0 ppm. If these systems are located in the hydrophobic chloroform dispersion medium, the organization of bound water strongly changes to reduce the contact area between immiscible liquids. Typically, chloroform can displace adsorbed water into narrow nanopores (inaccessible for larger chloroform molecules) or/and into larger pores (to reduce the contact area between them). In the systems studied, narrow pores give a minor contribution; therefore, chloroform displaces water mainly into larger pores. This results in a decrease in the amounts of SBW. A fraction of weakly associated water (δ_H = 1–2 ppm), *i.e.*, strongly clustered water with 1D and 2D structures, appears in PMS/A-300_{11} undergoing low mechanical loading. In PMS/A-300_{19} or after stronger mechanical loading on PMS/A-300_{11}, only strongly associated water is observed due to (i) a small content of hydrophobic functionalities in the former, or (ii) changes in the confined

space effects in more strongly compacted secondary particles for the latter.

If trifluoroacetic acid is added to the chloroform medium, the colligative and confined space effects overlap and the amount of SBW increases. Note that in this case, the changes in the porosity caused by the appearance of the ice crystallites in interparticle voids can be smaller than those in the systems with a main fraction of SAW/WBW.

The PMS/nanosilica blends at various weight ratio can be of interest from a practical point of view for applications as medical sorbents or preparation for agriculture applications [26, 27, 57]. The blends can be with improved or better controlled textural and adsorption characteristics, which can be easily varied in a broader range due to changes in composition and pretreatment conditions. Note that tests of these systems in various applications were started, and some promised results were obtained. In the future, it will be of interest to generalize the interfacial phenomena related to nanostructured blends of various hydrophilic and hydrophobic nanomaterials of various origin and nature.

Структурні та адсорбційні особливості аморфного нанокремнезему, модифікованого додаванням різної кількості поліметилсилоксану

В.В. Туров, В.М. Гунько, Т.В. Крупська, І.С. Процак, Є.М. Пахлов

Інститут хімії поверхні ім. О.О. Чуйка Національної академії наук України
вул. Генерала Наумова, 17, Київ, 03164, Україна, v_turov@ukr.net

Мета роботи полягала в детальному аналізі впливу поліметилсилоксану (ПМС) і умов підготовки на поведінку зв'язаної води, як і на властивості сумішей поліметилсилоксан/нанокремнезем. Аморфний нанокремнезем А-300 з добавкою гідрогелю ПМС (ПМС/А-300 = 1:9 для сухих компонентів) було вивчено в різних дисперсійних середовищах (повітря, хлороформ, чистий чи з додаванням трифтороцтової кислоти, TFAA) у порівнянні з ПМС та А-300 чи ПМС/А-300 (1:1) з використанням низькотемпературної ЯМР ^{1}H спектроскопії та кріопорометрії. Сухий А-300 та ПМС, окремо чи у сумішах, було вивчено за допомогою мікроскопії, адсорбції азоту, інфрачервоної спектроскопії та квантової хімії. Було показано, що властивості сумішей залежать не тільки від вмісту компонентів, але й механічного навантаження внаслідок більш сильного ущільнення вторинних структур наночастинок (агрегатів наночастинок та їх агломератів) при зростанні механічного навантаження. Слід зазначити, що таку поведінку різних сумішей гідрофобних та гідрофильних наноструктурованих матеріалів спостерігали після гідроущільнення з різнім навантаженням. Теоретичне моделювання показало, що будова зв'язаної води, яка локалізована на поверхні гідрофільних та гідрофобних наночастинок, змінюється при ущільненні агрегатів внаслідок змін впливу ефектів обмеженого простору та полярності молекул зв'язаної води. Ці результати відображають певну загальну закономірність, яка спостерігається в гібридних гідрофобних/гідрофільних системах при додаванні певної кількості води та при певному механічному навантаженні. Ці системи стають гідрофільними, проте після сушки вони знову можуть мати гідрофобні властивості, які знову зникають при повторному гідроущільненні.

Ключові слова: *нанокремнезем, поліметилсилоксан-гідрогель, поліметилсилоксан/нанокремнезем суміш, текстурні та морфологічні характеристики, вплив механічної обробки, поведінка міжфазної води*

Структурные и адсорбционные особенности аморфного нанокремнезема, модифицированного добавлением разного количества полиметилсилоксана

В.В. Туров, В.М. Гунько, Т.В. Крупская, И.С. Процак, Е.М. Пахлов

Институт химии поверхности им. А.А. Чуйко Национальной академии наук Украины
ул. Генерала Наумова, 17, Киев, 03164, Украина, v_turov@ukr.net

Цель роботы состояла в детальном анализе влияния полиметилсилоксана (ПМС) и условий подготовки на поведение связанной воды, как и на свойства смесей полиметилсилоксан/нанокремнезем. Аморфный нанокремнезем А-300 с добавкой гидрогеля ПМС (ПМС/А-300 = 1:9 для сухих компонентов) был изучен в разных дисперсионных средах (воздух, хлороформ, чистый или с добавкой трифторуксусной кислоты) по сравнению с ПМС и А-300 или ПМС/А-300 (1:1) с использованием низкотемпературной ЯМР ^{1}H спектроскопии и криопорометрии. Сухой А-300 и ПМС, отдельно или в смесях, были изучены с помощью микроскопии, адсорбции азота, инфракрасной спектроскопии и квантовой химии. Было показано, что свойства смесей зависят не только от содержания компонентов, но и от механической нагрузки вследствие более сильного уплотнения вторичных структур наночастиц (агрегатов наночастиц и их агломератов) при увеличении механической нагрузки. Следует отметить, что такое поведение разных смесей гидрофобных и гидрофильных наноструктурированных материалов наблюдали после гидроуплотнения при различных нагрузках. Теоретическое моделирование показало, что строение связанной воды, локализованной на поверхности гидрофильных и гидрофобных наночастиц, изменяется при уплотнении агрегатов вследствие изменений влияния эффектов ограниченного пространства и полярности молекул связанной воды. Эти результаты отражают некоторую общую закономерность, которая наблюдается в гибридных гидрофобных/гидрофильных системах при добавлении некоторого количества воды и при некоторой механической нагрузке. Эти системы становятся гидрофильными, хотя после сушки они снова могут иметь гидрофобные свойства, которые снова исчезают при повторном гидроуплотнении.

Ключевые слова: *нанокремнезем, полиметилсилоксан-гидрогель, полиметилсилоксан/нанокремнезем смесь, текстурные и морфологические характеристики, влияние механической обработки, поведение межфазной воды*

REFERENCES

1. *Ullmann's Encyclopedia of Industrial Chemistry*. (Weinheim: Wiley-VCH, 2008).
2. Büchel K.H., Moretto H.-H., Woditsch P. *Industrial Inorganic Chemistry*. (Weinheim Wiley-VCH, 2000).
3. Auner N., Weis J. *Oganosilicon Chemistry VI*. (Weinheim: Wiley-VCH, 2005).
4. *Basic Characteristics of Aerosil. Technical Bulletin Pigments*. N 11. (Hanau: Degussa AG, 1997).
5. Iler R.K. *The Chemistry of Silica*. (Chichester: Wiley, 1979).
6. Legrand A.P. *The Surface Properties of Silicas*. (New York: Wiley, 1998).
7. Vansant E.F., Van Der Voort P., Vrancken K.C. *Characterization and Chemical Modification of the Silica Surface: Studies in Surface Science and Catalysis*. V. 93. (Amsterdam: Elsevier, 1995).
8. Chuiko A.A. *Chemistry of Silica Surface*. (Kiyv: UkrINTEI, 2001). [in Russian].
9. Chuiko A.A. *Medical Chemistry and Clinical Application of Silicon Dioxide*. (Kiyv: Naukova Dumka, 2003). [in Russian].
10. Cai Y., Li J., Yi L., Yan X., Li J. Fabricating superhydrophobic and oleophobic surface with silica nanoparticles modified by silanes and environment-friendly fluorinated chemicals. *Appl. Surf. Sci.* 2018. **450**: 102.
11. Zhu Y., Chen L., Zhang C., Guan Z. Preparation of hydrophobic antireflective SiO2 coating with deposition of PDMS from water-based SiO_2-PEG sol. *Appl. Surf. Sci.* 2018. **457**: 522.
12. Zhao Y., Wen J., Ge Y., Zhang X., Shi H., Yang K., Gao X., Shi S., Gong Y. Fabrication of stable biomimetic coating on PDMS surface: Cooperativity of multivalent interactions. *Appl. Surf. Sci.* 2019. **469**: 720.
13. Conti J., De Coninck J., Ghazzal M.N. Design of water-repellant coating using dual scale size of hybrid silica nanoparticles on polymer surface. *Appl. Surf. Sci.* 2018. **436**: 234.
14. Ghosh S.K. *Functional Coatings*. (Weinheim: Wiley-VCH Verlag GmbH, 2006).
15. Bergna H.E., Roberts W.O. *Colloidal Silica: Fundamentals and Applications*. (Boca Raton: CRC Press, 2006).

16. Protsak I.S., Henderson I.M., Tertykh V.A., Dong W., Le Z. Cleavage of organosiloxanes with dimethyl carbonate: a mild approach to graft-to-surface modification. *Langmuir.* 2018. **34**(33): 9719.
17. Slinyakova B., Denisova T.I. *Organosilicon Adsorbents: Preparation and Properties*. (Kiyv: Naukova Dumka, 1988). [in Russian].
18. Wu L., Baghdachi J. *Functional Polymer Coatings: Principles, Methods, and Applications. First Edition*. (New York: John Wiley & Sons, 2015).
19. Gun'ko V.M., Turov V.V. *Nuclear Magnetic Resonance Studies of Interfacial Phenomena*. (Boca Raton: CRC Press, 2013).
20. Voronin E.F., Gun'ko V.M., Guzenko N.V., Pakhlov E.M., Nosach L.V., Malysheva M.L., Skubiszewska-Zięba J., Leboda R., Borysenko M.V., Chuiko A.A. Interaction of poly(ethylene oxide) with fumed silica. *J. Colloid Interface Sci*. 2004. **279**(2): 326.
21. Gun'ko V.M., Leboda R., Skubiszewska-Zięba J., Goncharuk E.V., Nychiporuk Y.M., Zarko V.I., Blitz J.P. Influence of different treatments on characteristics of nanooxide powders alone or with adsorbed polar polymers or proteins. *Powder Technology*. 2008. **187**(2): 146.
22. Gun'ko V.M., Turov V.V., Krupska T.V., Protsak I.S., Borysenko M.V., Pakhlov E.M. Polymethylsiloxane alone and in composition with nanosilica under various conditions. *J. Colloid Interface Sci.* 2019. **541**: 213.
23. Gun'ko V.M., Pakhlov E.M., Goncharuk O.V., Andriyko L.S., Nychiporuk Yu.M., Balakin D.Yu., Sternik D., Derylo-Marczewska A. Nanosilica modified by polydimethylsiloxane depolymerized and chemically bound to nanoparticles or physically bound to unmodified or modified surfaces: Structure and interfacial phenomena. *J. Colloid Interface Sci.* 2018. **529**: 273.
24. Gun'ko V.M. *Polymer composites with functionalized silica. In: Polymer Composites with Functionalized Nanoparticles. Synthesis, Interactions*. (Properties and Applications, Elsevier, 2018).
25. Mark J.E., Allcock H.R., West R. *Inorganic Polymers, Prentice Hall*. (New York: Englewood, 1992).
26. Nikolaev V.G. Enterosgel: A novel organosilicon enterosorbent with a wide range of medical applications. In: *Biodefence. Advanced Materials and Methods for Health Protection*. (Dordrecht: Springer, 2011).
27. Shevchenko Yu.N., Dushanin B.M., Yashinina N.I. New silicon compounds - porous organosilicon materials for technology and medicine. *Silicon for the Chemistry Industry III*. (Sandefjord, Norway, 1996).
28. Lotters J.C., Olthuis W., Veltink P.H., Bergveld P. The mechanical properties of the rubber elastic polymer polydimethylsiloxane for sensor applications. *J. Micromech. Microeng*. 1997. **7**(3): 145.
29. McDonald J.C., Duffy D.C., Anderson J.R., Chiu D.T., Wu H., Schueller O.J.A., Whitesides G.M. Fabrication of microfluidic systems in poly(dimethylsiloxane). *Electrophoresis.* 2000. **21**(1): 27.
30. Fadeev A.Y., Kazakevich Y.V. Covalently attached monolayers of oligo(dimethylsiloxane)s on silica: A siloxane chemistry approach for surface modification. *Langmuir.* 2002. **18**(7): 2665.
31. Litvinov V.M., Barthel H., Weis J. Structure of a PDMS layer grafted onto a silica surface studied by means of DSC and solid-state NMR. *Macromolecules.* 2002. **35**(11): 4356.
32. Gun'ko V.M., Turov V.V., Zarko V.I., Goncharuk E.V., Gerashchenko I.I., Turova A.A., Mironyuk I.F., Leboda R., Skubiszewska-Zięba J., Janusz W. Comparative characterization of polymethylsiloxane hydrogel and silylated fumed silica and silica gel. *J. Colloid Interface Sci.* 2007. **308**(1): 142.
33. Finiels A., Alonso B., Bousmina M., Brunel D., El Kadib A. Periodic mesoporous organosilicas derived from amphiphilic bulky polymethylsiloxane. *New J. Chem.* 2016. **40**(5): 4132.
34. Li Y., Luo C., Li X., Zhang K., Zhao Y., Zhu K. Submicron / nano-structured icephobic surfaces made from fluorinated polymethylsiloxane and octavinyl-POSS. *Appl. Surf. Sci.* 2016. **360**: 113.
35. Li F., Ji C., Yun Z. Synthesis of alkyl polymethylsiloxane (APMS) by condensation reaction and study of properties as lubricants. *J. Macromol. Sci. Part A Pure Appl. Chem.* 2018. **55**(4): 332.
36. Nagappan S., Joo J., Soo S., Hong S., Sik Y. Polymethylhydrosiloxane-based organic – inorganic hybrids for amphiphobic coatings. *Compos. Interfaces.* 2013. **20**(1): 33.
37. Sharaf M.A., Mark J.E. Modulus of randomly crosslinked polymethysiloxane networks, Polymeric Materials Science and Engineering. *Proc. ACS Division of Polymeric Materials Science and Engineering*. 1993. **68**: 180.
38. Shimizu T., Kanamori K., Maeno A., Kaji H., Nakanishi K. Transparent ethylene-bridged polymethylsiloxane aerogels and xerogels with improved bending flexibility. *Langmuir.* 2016. **32**(50): 13427.
39. Shimizu T., Kanamori K., Maeno A., Kaji H., Doherty C.M. Transparent ethenylene-bridged polymethylsiloxane aerogels: mechanical flexibility and strength and availability for addition reaction. *Langmuir.* 2017. **33**(18): 4543.
40. Zhang H., Lana C., Ana F., Teixeira L., Michaela S. Water-based freeze casting: Adjusting hydrophobic polymethylsiloxane for obtaining hierarchically ordered porous SiOC. *J. Am. Ceram. Soc.* 2017. **100**(5): 1907.
41. Zu G., Shimizu T., Kanamori K., Zhu Y., Maeno A., Kaji H., Shen J., Nakanishi K. Transparent, super flexible doubly cross- linked polyvinylpolymethylsiloxane aerogel superinsulators via ambient pressure drying. *ACS Nano.* 2018. **12**(1): 521.

42. Michurina S.V., Ischenko I.Y., Arkhipov S.A., Klimontov V.V, CherepanovaM.A., Korolev M.A., Rachkovskaya L.N., Zav E.L., Konenkov V.I. Melatonin − aluminum oxide – polymethylsiloxane complex on apoptosis of liver cells in a model of obesity and type 2 diabetes mellitus. *Bulletin of Experimental Biology and Medicine.* 2017. **164**: 165.
43. Gun'ko V.M., Turov V.V., Pakhlov E.M., Matkovsky A.K., Krupska T.V., Kartel M.T., Charmas B. Blends of amorphous/crystalline nanoalumina and hydrophobic amorphous nanosilica. *J. Non-Cryst. Solids.* 2018. **500**: 351.
44. Gun'ko V.M., Turov V.V., Pakhlov E.M., Krupska T.V., Borysenko M.V., Kartel M.T., Charmas B. Water interactions with hydrophobic versus hydrophilic nanosilica. *Langmuir.* 2018. **34**(12): 12145.
45. Gun'ko V.M., Turov V.V., Krupska T.V., Pakhlov E.M. Behavior of water and methane bound to hydrophilic and hydrophobic nanosilicas and their mixture. *Chem. Phys. Lett.* 2017. **690**: 25.
46. Turov V.V., Gun'ko V.M., Pakhlov E.M., Krupska T.V., Tsapko M.D., Charmas B., Kartel M.T. Influence of hydrophobic nanosilica and hydrophobic medium on water bound in hydrophilic components of complex systems. *Colloids Surf. A.* 2018. **552**: 39.
47. Gregg S.J., Sing K.S.W. *Adsorption, Surface Area and Porosity*. (London: Academic Press, 1982).
48. Adamson A.W., Gast A.P. *Physical Chemistry of Surface*. 6th edition. (New York: Wiley, 1997).
49. Neimark A.V., Ravikovitch P.I. Capillary condensation in MMS and pore structure characterization. *Microporous Mesoporous Mater.* 2001. **44/45**: 697.
50. Gun'ko V.M. Composite materials: textural characteristics. *Appl. Surf. Sci.* 2014. **307**: 444.
51. Strange J.H., Rahman M., Smith E.G. Characterization of porous solids by NMR. *Phys. Rev. Lett.* 1993. **71**: 3589.
52. Mitchell J., Webber J.B.W., Strange J.H. Nuclear magnetic resonance cryoporometry. *Phys. Rep.* 2008. **461**: 1.
53. Petrov O.V., Furó I. NMR cryoporometry: Principles, applications and potential. *Prog. Nucl. Magn. Reson. Spectrosc.* 2009. **54**(2): 97.
54. Frisch M.J., Trucks G.W., Schlegel H.B., Scuseria G.E., Robb M.A., Cheeseman J.R., Scalmani G., Barone V., Mennucci B., Petersson G.A., Nakatsuji H., Caricato M., Li X., Hratchian H.P., Izmaylov A.F., Bloino J., Zheng G., Sonnenberg J.L., Hada M., Ehara M., Toyota K., Fukuda R., Hasegawa J., Ishida M., Nakajima T., Honda Y., Kitao O., Nakai H., Vreven T., Montgomery J.A., Jr., Peralta J.E., Ogliaro F., Bearpark M., Heyd J.J., Brothers E., Kudin K.N., Staroverov V.N., Keith T., Kobayashi R., Normand J., Raghavachari K., Rendell A., Burant J.C., Iyengar S.S., Tomasi J., Cossi M., Rega N., Millam J.M., Klene M., Knox J.E., Cross J.B., Bakken V., Adamo C., Jaramillo J., Gomperts R., Stratmann R.E., Yazyev O., Austin A.J., Cammi R., Pomelli C., Ochterski J.W., Martin R.L., Morokuma K., Zakrzewski V.G., Voth G.A., Salvador P., Dannenberg J.J., Dapprich S., Daniels A.D., Farkas O., Foresman J.B., Ortiz J.V., Cioslowski J., Fox D.J. Gaussian 09, Revision D.01, Gaussian, Inc., Wallingford CT, 2013.
55. Stewart J.J.P. MOPAC2016, Stewart Computational Chemistry. 2017. http://OpenMOPAC.net.
56. Stewart J.J.P. Optimization of parameters for semiempirical methods VI: more modifications to the NDDO approximations and re-optimization of parameters. *J. Mol. Model.* 2013. **19**(1): 1.
57. Zhurko G.A., Zhurko D.A. Chemcraft (version 1.8, build b536a). 2017. http://www.chemcraftprog.com.
58. Hanwell M.D., Curtis D.E., Lonie D.C., Vandermeersch T., Zurek E., Hutchison G.R. Avogadro: an advanced semantic chemical editor, visualization, and analysis platform. *J. Chem. Inform.* 2012. **4**(1): 17.
59. Emsley J.W., Feeney J., Sutcliffe L.H. *High Resolution Nuclear Magnetic Resonance Spectroscopy*. (Oxford: Pergamon Press, 1965).
60. Chaplin M. Water structure and science. 2018. http://www1.lsbu.ac.uk/water/.
61. Gun'ko V.M., Turov V.V., Pakhlov E.M., Krupska T.V., Charmas B. Effect of water content on the characteristics of hydro-compacted nanosilica. *Appl. Surf. Sci.* 2018. **459**: 171.
62. Turov V.V., Geraschenko I.I., Krupska T.V., Suvorova L. *Nanochemistry in solution of problems of exo- and endo-ecology*. (Stavropol: Zebra, 2017). [in Russian]).
63. Mikheev Yu.A., Guseva L.N., Davydov E.Ya., Ershov Yu.A. The hydration of hydrophobic substances. *Russ. J. Phys. Chem.* 2007. **81**(12): 1897.
64. Yaminsky V.V., Vogler E.A. Hydrophobic hydration. *Current Opinion in Colloid & Interface Science.* 2001. **6**(4): 342.
65. Widom B., Bhimalapuram P., Koga K. The hydrophobic effect. *Phys. Chem. Chem. Phys*. 2003. **5**(15): 3085.

Received 04.04.2019, accepted 20.08.2019